



Water Resources Research

RESEARCH ARTICLE

10.1029/2020WR028193

Key Points:

- Climate warming expands the erodible landscape and increases fluvial water and sediment fluxes on the Tibetan Plateau
- Air temperature regulates seasonal discharge and sediment dynamics by controlling glacier-snow melt and permafrost processes
- Increasing rainstorms results in more frequent fluvial extreme events

Supporting Information:

• Figure S1

Correspondence to:

X. Lu and D. Li, geoluxx@nus.edu.sg; dongfeng@u.nus.edu

Citation:

Li, D., Overeem, I., Kettner, A. J., Zhou, Y., & Lu, X. (2021). Air temperature regulates erodible landscape, water, and sediment fluxes in the permafrost-dominated catchment on the Tibetan Plateau. *Water Resources Research*, 57, e2020WR028193. https://doi.org/10.1029/2020WR028193

Received 17 JUN 2020 Accepted 23 DEC 2020

Air Temperature Regulates Erodible Landscape, Water, and Sediment Fluxes in the Permafrost-Dominated Catchment on the Tibetan Plateau

Dongfeng Li¹, Irina Overeem², Albert J. Kettner², Yinjun Zhou³, and Xixi Lu^{1,4}

¹Department of Geography, National University of Singapore, Kent Ridge, Singapore, ²CSDMS, Institute of Arctic and Alpine Research, University of Colorado Boulder, Boulder, CO, USA, ³Changjiang River Scientific Research Institute, Wuhan, China, ⁴Inner Mongolian Key Lab of River and Lake Ecology, School of Ecology and Environment, University of Inner Mongolia, Hohhot, China

Abstract Approximately 40% of the Tibetan Plateau (TP) is underlain by continuous permafrost, yet its impact on fluvial water and sediment dynamics remains poorly investigated. Here we show that water and sediment dynamics in the permafrost-dominated Tuotuohe basin on the TP are driven by air temperature and permafrost thaw, based on 33-year daily in situ observations (1985-2017). Air temperature regulates the seasonal patterns of discharge and suspended sediment concentration (SSC) by controlling the changes in active contributing drainage area (ACDA, the unfrozen erodible landscape that contributes hydrogeomorphic processes within a catchment) and governing multiple thermal processes such as glacier-snow melt and permafrost thaw. Rainstorms determine the short-lived fluvial extreme events by intensifying slope processes and channel erosion and likely also by enhancing thaw slumps. Furthermore, the SSCs at equal levels of discharges are lower in autumn (September-October) than in spring (May-June) and summer (July-August). This reduced sediment availability in autumn can possibly be attributed to the increased supra-permafrost groundwater runoff and the reduced surface runoff and erosion. Due to rapid climate warming, the ACDA has increased significantly from 1985 to 2017, implying expanding erodible landscapes for hydrogeomorphic processes. As a result, the fluvial water and sediment fluxes have substantially increased. In a warmer and wetter future for the TP, the fluvial sediment fluxes of similar permafrost-underlain basins will continue to increase with expanding erodible landscapes and intensifying thermal and pluvial-driven geomorphic processes. Thus, permafrost thaw should be considered as an important driver of past and future water and sediment changes for the TP.

1. Introduction

The high-altitude Tibetan Plateau (TP) has the planet's third largest cryosphere reservoir (glacier-snow-permafrost) and is highly sensitive to global climate change (Immerzeel et al., 2020, 2010; Yao et al., 2019). Since the 1950s, the average air temperature on the TP has warmed 1.9°C at a rate of 0.32°C per decade, which is twice of the global average warming rate (IPCC, 2019). In response to such rapid warming, glaciers have been retreated at a rate of 16.3 ± 3.5 Gt yr⁻¹ over 2000 to 2016 (Brun et al., 2017) and the snow water equivalent overall exhibits a negative trend especially in mid-elevation areas (Smith & Bookhagen, 2018). More importantly, the TP contains the world's largest area of alpine permafrost ($\sim 1.3 \times 10^6 \text{ km}^2 \text{ or } 42\% \text{ of the TP}$) (T. Wang et al., 2020). Permafrost degradation on the TP is now accelerating and the active layer thickness (thickness of the top layer of soil that seasonally thaws) is increasing at a rate faster than in pan-Arctic regions (Biskaborn et al., 2019; T. Wang et al., 2020). Glacier and snow mass losses have been found to affect the seasonal and annual streamflow and water supply of the TP rivers, but the impact of permafrost thaw has been largely overlooked by prior studies (Huss & Hock, 2018; Immerzeel et al., 2020, 2010; Zhao et al., 2019). Additionally, the response of fluvial sediment transport to climatic and cryospheric changes on the TP remains much less investigated, compared with the many studies on streamflow in the region (IPCC, 2019). This is despite the fact that sediment often carries nutrients, heavy metals, and organic carbon and significantly influences water quality, aquatic ecosystems, agriculture, and thus millions of peoples living in the downstream areas (Best, 2019; Lu et al., 2010; Milliman & Syvitski, 1992; Syvitski, 2002; Walling, 2006).

The impact of a changing climate and cryosphere on riverine sediment is complex as it involves sediment production, transport, and storage via multiple processes such as glacier retreat, proglacial activity, slope

© 2021. American Geophysical Union. All Rights Reserved.

LI ET AL.



and permafrost processes, channel erosion, and floodplain deposition (Dietrich & Dunne, 1978; Lane et al., 2017). Our limited process understanding of sediment transport in cold environments is partly due to absence of quantitative data, particularly long-term in situ monitoring data (longer than 10 years) (Beel et al., 2018; Beylich et al., 2017). Recent research progress on glacier retreat, permafrost disturbance, and sediment production from polar regions and the European Alps has shed some light on such impacts (Beel et al., 2018; Delaney & Adhikari, 2020; Kokelj et al., 2013; Koppes et al., 2015; Overeem et al., 2017; Rudy et al., 2017). For instance, increasing fluvial sediment and nutrient fluxes following permafrost disturbance have been observed in the Canadian Arctic (Kokelj et al., 2013; Rudy et al., 2017). Yet, how the riverine sediment dynamics are controlled by temperature and permafrost processes is unknown for the many permafrost-underlain river basins of the TP, where the active layers are generally thicker and the terrains are much steeper than in the polar regions (T. Wang et al., 2020).

A few studies have investigated permafrost runoff processes and their relations with temperature and precipitation based on several consecutive years' of in situ observations on the TP (G. Wang et al., 2012, 2009). They confirmed that the soil water dynamics are mainly driven by temperature rather than precipitation and the active layer freeze-thaw variation determines seasonal water budget. The surface soil water content increases with active layer thaw from spring to summer and may decrease in autumn when the active layer reaches its maximum depth (Q. Wang, Zhang, et al., 2017). Furthermore, the supra-permafrost water (groundwater that is mainly stored in active layer) plays a dominant role in the total runoff during autumn recession season for many permafrost catchments on the TP (Z. Li, Li, Feng, et al., 2020; G. Wang et al., 2009). Nevertheless, the impacts of these seasonal freeze-thaw cycles on sediment dynamics have not been examined.

This study analyzes 33 years (1985–2017) of daily in situ observations of discharge, suspended sediment concentration (SSC), and suspended sediment flux (SSF, the product of discharge and SSC), from a pristine (without human interventions) basin on the TP, and examines the responses of riverine sediment to climate change and permafrost thaw. The selected Tuotuothe (TTH) basin has an area of \sim 18,000 km² and is underlain by continuous permafrost with 2% of the area being glacierized (Figure 1). Here, we investigate how air temperature and precipitation control the discharge and sediment dynamics through the evolving erodible landscape (i.e., active contributing drainage area [ACDA]), active layer freeze-thaw, and multiple thermal/pluvial processes in the permafrost-underlain basin on the TP. The implications for fluvial dynamics in a future warmer and wetter TP are also discussed.

2. Materials and Methods

2.1. Geographical Setting

The TTH basin, located in central-eastern TP, is the most remote headwater river of the Yangtze River (Figure 1). The TTH basin receives its moisture mostly from the East Asian monsoon, with >90% of the annual total precipitation falling from May to October (Figure 1d). The TTH river has a length of \sim 350 km from the upstream glacier zone to the TTH hydrometeorological station, draining a catchment area of ~18,000 km². Glaciers span 380 km² (glacier coverage is 2%) and store an estimated volume of freshwater of ~42 km³ (Q. Wang, Zhang, et al., 2017). These glaciers predominantly melt in summer and provide $\sim 10\%$ of the total annual runoff (Shiyin et al., 2009; Q. Wang, Zhang, et al., 2017). The TTH basin is underlain by continuous ice-rich permafrost (98%) (Z. Li, Li, Feng, et al., 2020). Thaw of the active layer starts in May and ends in September and the maximum active layer thickness for the TTH basin ranges from 2.5 to 3.2 m (T. Wang et al., 2020). From October until April, the basin is frozen (R. Wang, Yao, et al., 2017). Supra-permafrost groundwater is thought to be the dominant source of runoff in the TTH basin (Z. Li, Li, Feng, et al., 2020). The vegetation in the TTH basin mainly comprises sparse grassland, with the mean monthly Normalized Difference Vegetation Index (NDVI) ranging from 0.1 to 0.23 (Supplement Figure S1). Furthermore, the TTH region is a pristine headwater basin with negligible human activities. There is only one small town at the basin outlet, Tangula (34.22 N, 92.44 E), with ~1,300 local Tibetan inhabitants. The undisturbed environment provides a unique opportunity to assess the impacts of climate change on fluvial processes in naturally changing systems.

Geologically, the TTH basin comprises mesozoic clastic sedimentary rocks such as conglomerates, sandstones, siltstones, and claystones (Y. Li et al., 2011; W. Wu et al., 2011). Moraines deposited since the last

LI ET AL. 2 of 14

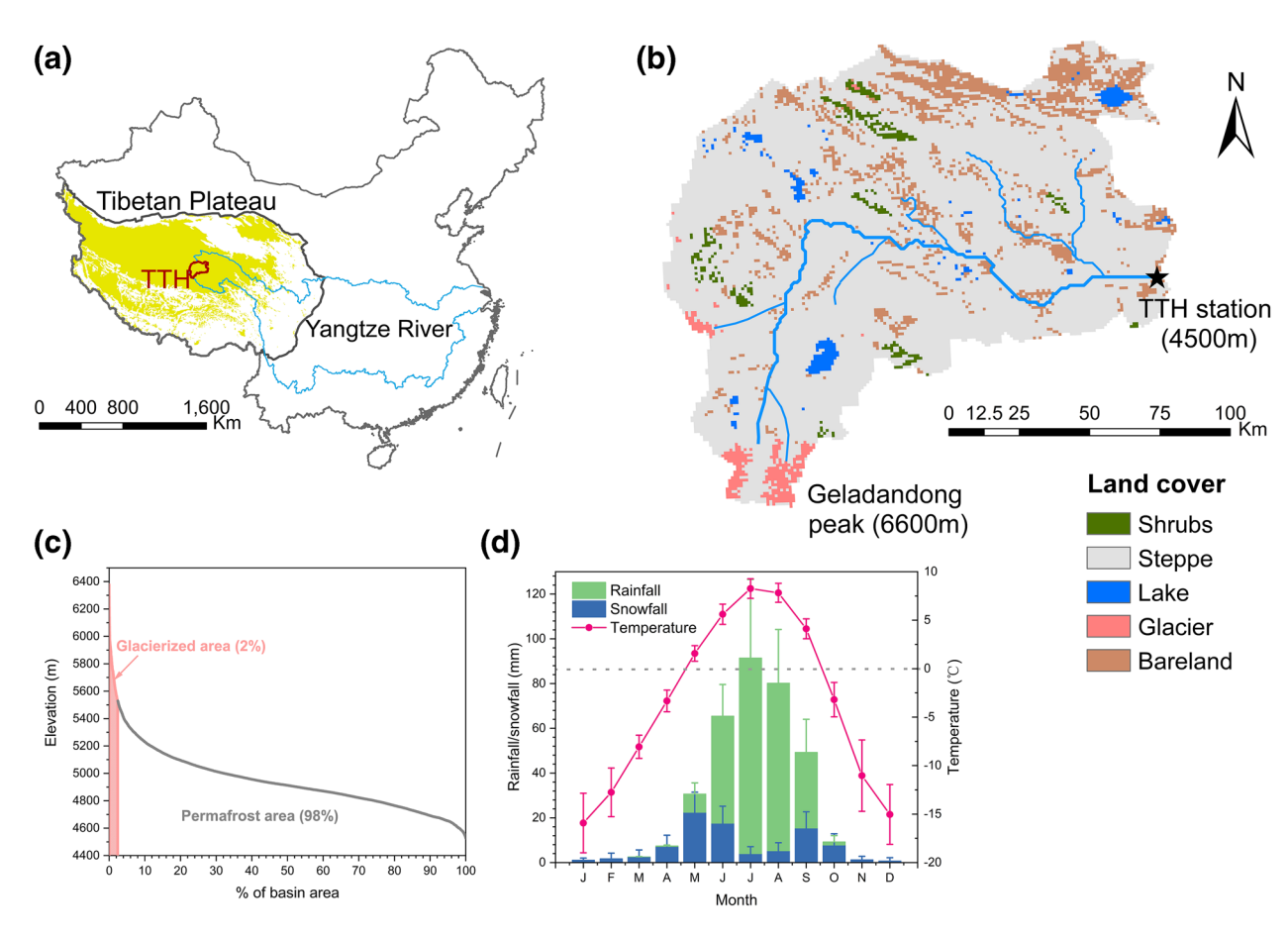


Figure 1. Basic characteristics of the Tuotuohe (TTH) basin on the central Tibetan Plateau (TP). (a) Permafrost distribution (yellow shaded area) on the TP and the location of the TTH basin. (b) Land cover in the TTH basin (GlobeLand30 data set; http://www.globallandcover.com). Main land cover is alpine steppe. The glacier coverage is small (2%) and all remaining area comprises continuous permafrost. (c) The hypsometric curve, showing accumulated area versus elevation distribution (SRTM DEM data set; http://srtm.csi.cgiar.org/srtmdata/). The glacierized area is located just above 5,500 m altitude. The upstream high-altitude glaciers are engaged into the erodible landscape when temperature at the TTH station exceeds ~6°C (assuming a lapse rate of 6°C/km). (d) Mean monthly rainfall, snowfall, and air temperature. Rainfall and snowfall are separated using a temperature threshold method (Gunawardhana & Kazama, 2012).

glacial maximum are limited and occur in the upstream mountains (>5,000 m a.s.l.) (Colgan et al., 2006). The river channels are characterized by sand-gravel bed braided rivers with well-developed floodplains (>5 km width near the TTH station). Since the TTH basin is underlain by ice-rich permafrost with limited glacial environments in the upstream mountains, the main thermally induced sediment sources include thaw slumps, thermal gullies, snowmelt erosion, and glacial erosion (Figures 2 and 3). In particular, the mega-scale thaw slumps that are coupled with channels could be important sediment supplies (Figure 2c). Conventional erosional processes such as slope wash, mass wasting, and fluvial channel erosion are also important sediment sources (Figure 3).

For the TTH basin, a hydrological year can be divided into four seasons: spring snowmelt season (May–June), summer melt season (July–August), autumn recession season (September–October), and frozen winter season (November–April). Winter precipitation starts melting in early May when air temperature begins to exceed 0°C (Q. Wang, Zhang, et al., 2017). The thaw cycle of frozen soil also initiates in May, but the thaw depth of the active layer in spring is shallow because of the low temperature and the snow cover (R. Wang, Yao, et al., 2017). Snowmelt dominates the hydrological processes in spring (Supplement Figure S1a). The highest temperature and precipitation occur throughout the summer, supporting a continuous increase in thaw depth. The active layer thaw depth reaches its maximum in September, and then it gradually decreases in October when the freeze cycle begins (R. Wang, Yao, et al., 2017).

LI ET AL. 3 of 14

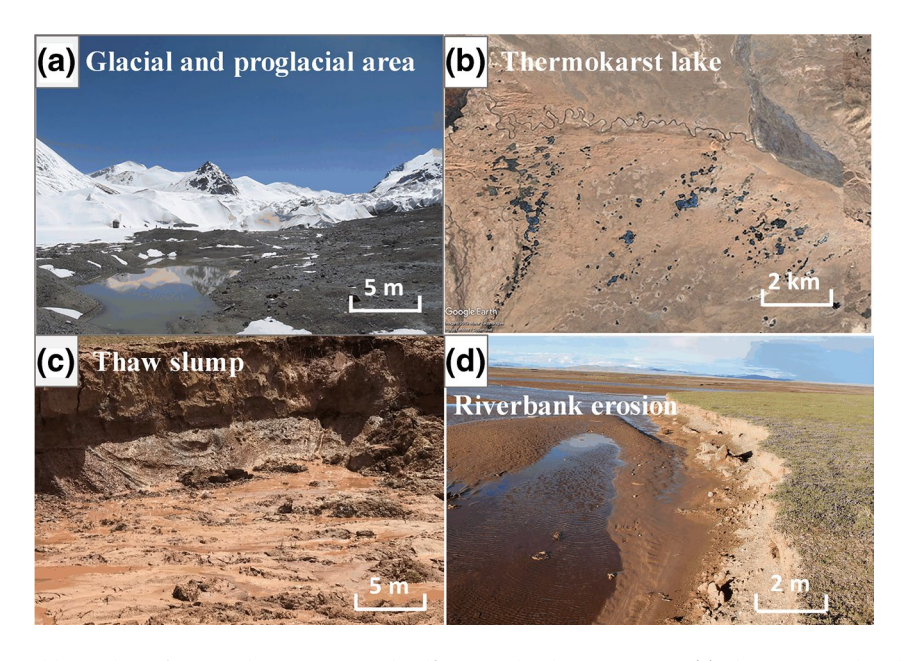


Figure 2. Field site photos/images showing various landforms and sediment sources. (a) The Gangjiaquba Glacier (the largest glacier in the TTH basin) and its proglacial areas (Photo by Y. Zhou). (b) Thermokarst lakes (evidence of ice-rich permafrost) on the floodplains (Google earth image on December 31, 2016). (c) Permafrost thaw slumps near the riverbank at the adjacent Beiluhe region (Photo by L. Huang). (d) Riverbank erosion, the well-developed floodplain, and sand-gravel riverbed near the TTH station (Photo by D. Li).

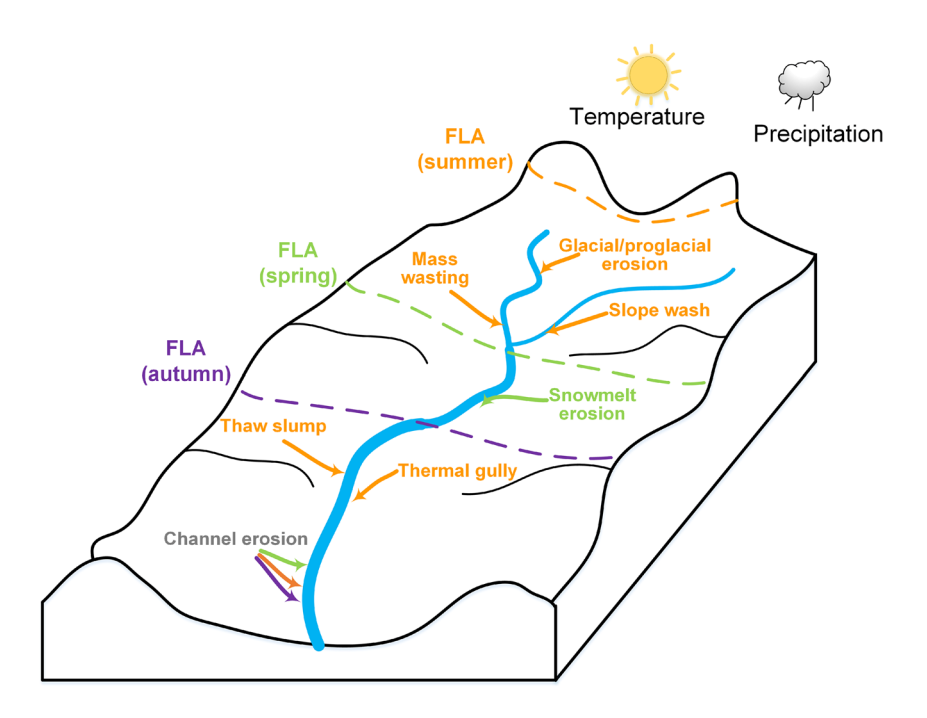


Figure 3. Conceptual depiction of the potential sediment sources across different seasons in the TTH basin. FLA = freezing line altitude. The drainage area below FLA (dotted lines) denotes the active erodible landscape or the ACDA that dominates runoff and sediment processes within the catchment. Snowmelt erosion mainly occurs in spring. In summer, there are multiple thermal erosions (glacial erosion, thaw slump, and thermal gully) and pluvial erosions (slope wash and mass wasting). Channel erosion can occur in spring, summer, and autumn.

LI ET AL. 4 of 14



2.2. Active Contributing Drainage Area

Inspired by the concept of saturated area that governs major hydrological and geomorphological processes within a catchment (Dunne & Black, 1970), we introduce the concept of an ever-evolving erodible landscape for cold mountainous environments. The erodible landscapes refer to the most relevant landscapes (e.g., active glaciers, permafrost slopes, and fluvial channels) that contribute runoff and sediment processes within a catchment. In cold mountainous environments, the erodible landscape is not a static topographically controlled entity; it evolves with seasonal variations in temperature. We further propose a simple proxy, "active contributing drainage area (ACDA)", to quantify the area of erodible landscape. We define the ACDA as the part of the total drainage area that is below the freezing line altitude (FLA, the altitude at which the air temperature is 0°C) for a given day. This definition assumes that thermal and pluvial processes of runoff and sediment transport dominantly occur in unfrozen landscapes (temperature is above 0°C) and thus the ADCA of a cold region evolves with fluctuations in temperature. Naturally, there may be lags in the system, where a set of warm days is being followed by a distinct cold spell (Beylich et al., 2017; Z. Li, Li, Feng, et al., 2020). However, such lags are filtered by using monthly mean ACDA. The ACDA is highly relevant to fluvial sediment flux because the magnitude of a river's sediment flux (Q_S) increases with its drainage area (A) ($Q_S = c A^d$; Milliman & Syvitski, 1992). For the TTH basin, the ACDA slowly increases in spring. When summer progresses, the ACDA reaches its maximum extent, followed by a strong receding trend throughout autumn and winter (Figure 3). Similarly, we can delineate the glaciated part of the catchment and to what extent it is contributing meltwater downstream based on the daily temperature.

Specifically, there are three steps to calculate the ACDA for a given day. First, if the air temperature (T) for a given day at the basin outlet (e.g., the TTH gauging station in this case) is below 0°C, then we assume the ACDA for the entire basin is zero. Second, if the T for a given day at the basin outlet exceeds 0°C, the FLA can be calculated as: FLA = H_0 + (T/L), where H_0 is the elevation of the basin outlet and L is the lapse rate (0.006°C/m in this case). Third, the ACDA is the sum of the total catchment areas below the FLA. Since the ACDA is a proxy that only accounts for air temperature and basin hypsometry, but does not consider the spatial heterogeneity of soil types and the potential impacts of vegetation and snow cover on permafrost freeze-thaw, we treat it as a maximum estimate of the erodible landscape within a catchment at any given day of the year. Also, ACDA only reflects the area of the erodible landscape and not the soil volume (i.e., both thaw area and thaw depth), which is affected when the ACDA expands and contracts.

2.3. Hydroclimate Data

The TTH gauging station is the most upstream hydrological station of the Yangtze River. It is located in a gravel-sand bed river reach and the monitored cross-section is overall stable. Daily mean water levels are recorded in nonfrozen seasons (i.e., May–October) as streamflow is near zero in other months. Daily mean discharges are calculated by the site-specific stage-discharge rating curves, which are calibrated over a wide range of discharge to ensure high accuracy ($R^2 > 0.95$). In case of flood events, discharge is measured more frequently. Daily SSC samples are collected by depth-integrating samplers (DH-48) at \sim 0,800 a.m. (Beijing Time). Normally, daily measurement of SSC is conducted, while more frequent, subdaily measurements (more than four times a day) are collected during the flood season when there is high variation of SSC. Daily mean SSC is estimated from a combination of point and depth-integrated measurements spanning the monitored cross-section of the channel with at least four sampling points along the cross-section. In the sediment laboratory, SSC samples are volumetrically filtered, oven-dried, and weighed. Daily mean sediment flux (kg/s) is calculated as the product of daily mean discharge (m³/s) and daily mean SSC (kg/m³). In addition, daily air temperature and precipitation are sourced from the National Meteorological Information Center, China Meteorological Administration.

3. Results

3.1. Interannual Variability of Erodible Landscape, Water, and Sediment Fluxes

In response to rapid climate warming and permafrost thawing, the active erodible landscape, represented by the ACDA, in the TTH basin is expanding (Figure 4). The annual mean ACDA is rising at a rate

LI ET AL. 5 of 14

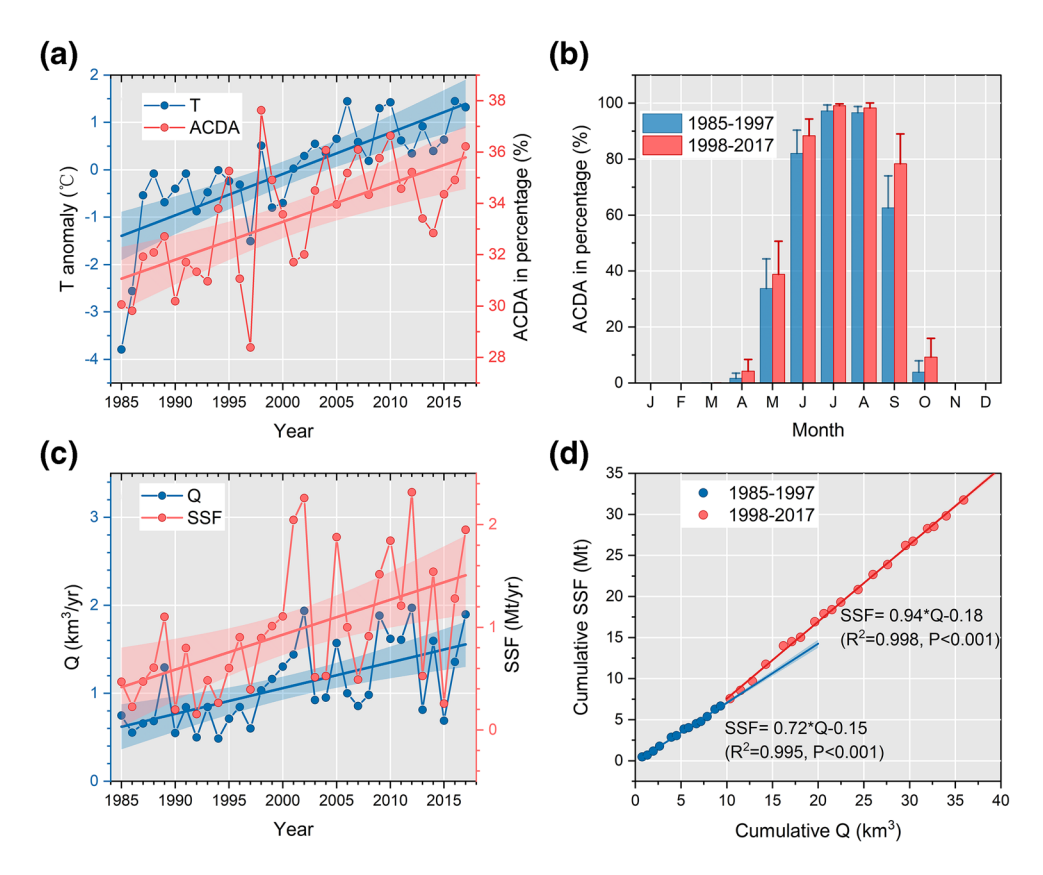


Figure 4. Expanding active contributing drainage area (ACDA) and increasing water and sediment fluxes. (a) Increases in the observed annual mean air temperature anomaly (T, slope = 0.08 ± 0.01 °C/yr, P < 0.001) and the annual mean ACDA (slope = 0.15 ± 0.03 %/yr, P < 0.001) from 1985 to 2017. (b) Increases in the mean monthly ACDA from 1985–1997 to 1998–2017. (c) Increases in the runoff (Q) and suspended sediment flux (SSF). (d) Double mass curves between cumulative SSF and cumulative Q, indicating a greater rise in SSF after 1997. The breakpoint (1997) is selected based on the Pettitt test (Pettitt, 1979), and corroborated by a climate regime shift on the TP after 1997 (D. Li, Li, Zhou, et al., 2020; Zhang et al., 2020). The shading area denotes 95% confidence interval.

of $0.15 \pm 0.03\%/yr$ (27.3 ± 5.5 km²/yr, P < 0.001) from 1985 to 2017. In particular, the ACDAs in spring (May–June) and autumn (September–October) exhibit large increases (5%–15% or 900–2,800 km²) during the period of 1998–2017, relative to the period of 1985–1997. Furthermore, the thaw season is extended (i.e., the total number of days with air temperatures exceeding 0°C increased by 12 days) from 1985–1997 to 1998–2017 (Supplement Figure S2). Meanwhile, the water and sediment fluxes have substantially increased at rates of $3.5 \pm 1\%/yr$ (0.029 ± 0.007 km³/yr) and $5.9 \pm 1.9\%/yr$ (0.034 ± 0.01 Mt/yr) over the period of 1985–2017, respectively (Figure 4c). Moreover, the sediment flux exhibits a greater rise than the runoff after 1997 as indicated by the Pettitt test and the double-mass-curve approach (Figure 4d).

3.2. Seasonal Variability of Erodible Landscape, Water, and Sediment Fluxes

The ACDA, discharge, SSC, and SSF in summer (July–August) are disproportionally higher than those in spring (May–June) and autumn (September–October, Figures 5 and 6). Over the entire investigation period from 1985 to 2017, 76% SSF (55% discharge) of the annual total is transported in summer, whereas 13% (18%) occurs in spring and 11% (27%) occurs in autumn (Figure 5). The median SSC in autumn (0.13 kg/m 3 in September and 0.05 kg/m 3 in October) is lower than that in spring (0.23 kg/m 3 in June and 0.20 kg/m 3 in May), while the median discharges in autumn (65.7 m 3 /s in September and 22 m 3 /s in October) are higher than those in spring (36.5 m 3 /s in June and 17.9 m 3 /s in May) (Figure 5). The monthly discharges, SSCs, and SSFs correspond closely to their ACDAs, suggesting the role of ACDA in governing the runoff and sediment generations in this permafrost-dominated catchment (Figure 6).

LI ET AL. 6 of 14

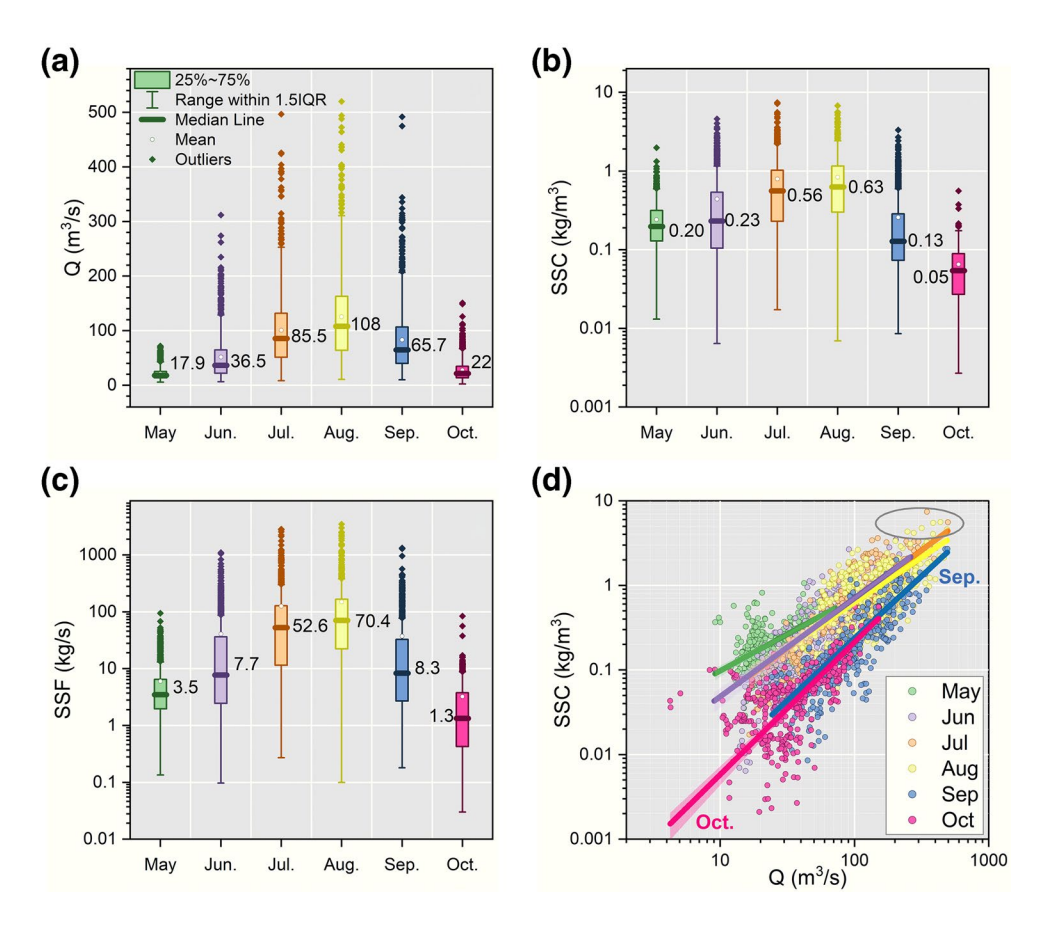


Figure 5. Discharge (Q), suspended sediment concentration (SSC), and suspended sediment flux (SSF) and Q-SSC relations from May to October. (a–c) Box-whisker plots of Q, SSC, and SSF in spring (May–June), summer (July–August), and autumn (September–October). The number adjacent to the box denotes the median value in each month. (d) Rating relations between discharge and SSC. Discharge-SSC relations in spring and summer differ significantly from those in autumn. Note that the most extreme SSC events (SSC $> 2.90 \text{ kg/m}^3$) occur during full summer conditions (see the orange and yellow dots in the gray circle in (d)). The shading area denotes 95% confidence interval.

The discharge-SSC relations in spring and summer exhibit different patterns from those in autumn (Figure 5d). The SSCs over the same discharge range of $10{\text -}100~\text{m}^3/\text{s}$ in spring and summer are higher than those in autumn, suggesting reduced sediment availability and sediment transport in autumn. In particular, the peak SSC events (SSC > $2.90~\text{kg/m}^3$ or the top 1 percentile of all the SSCs; Supplement Figure S3) only occur in summer (Figure 5d). At monthly timescale, the SSCs in May, June, July, and August are overall greater than those in September and October (Figure 6a). Higher variability in SSCs in July and August implies a more complex discharge-SSC relation and potentially multiple sediment sources during summer. The clockwise hysteresis loop between mean monthly discharge and mean monthly SSC points to a sediment supply limited system. Additionally, at the flood event timescale, sediment availability appears high during the rising stage but becomes exhausted during the falling stage. For instance, three of four successive floods in the late summer and early autumn of 2012 show this pattern (Figure 7). This highlights that high sediment transport capacity (i.e., high discharge) does not always produce equivalently high sediment concentrations in the permafrost-underlain basin.

4. Discussion

4.1. Thermal Control

We find that air temperature determines the seasonal pattern of fluvial water and sediment dynamics by controlling the ACDA and multiple thermal processes throughout the hydrological year (Figures 6 and 8

LI ET AL. 7 of 14

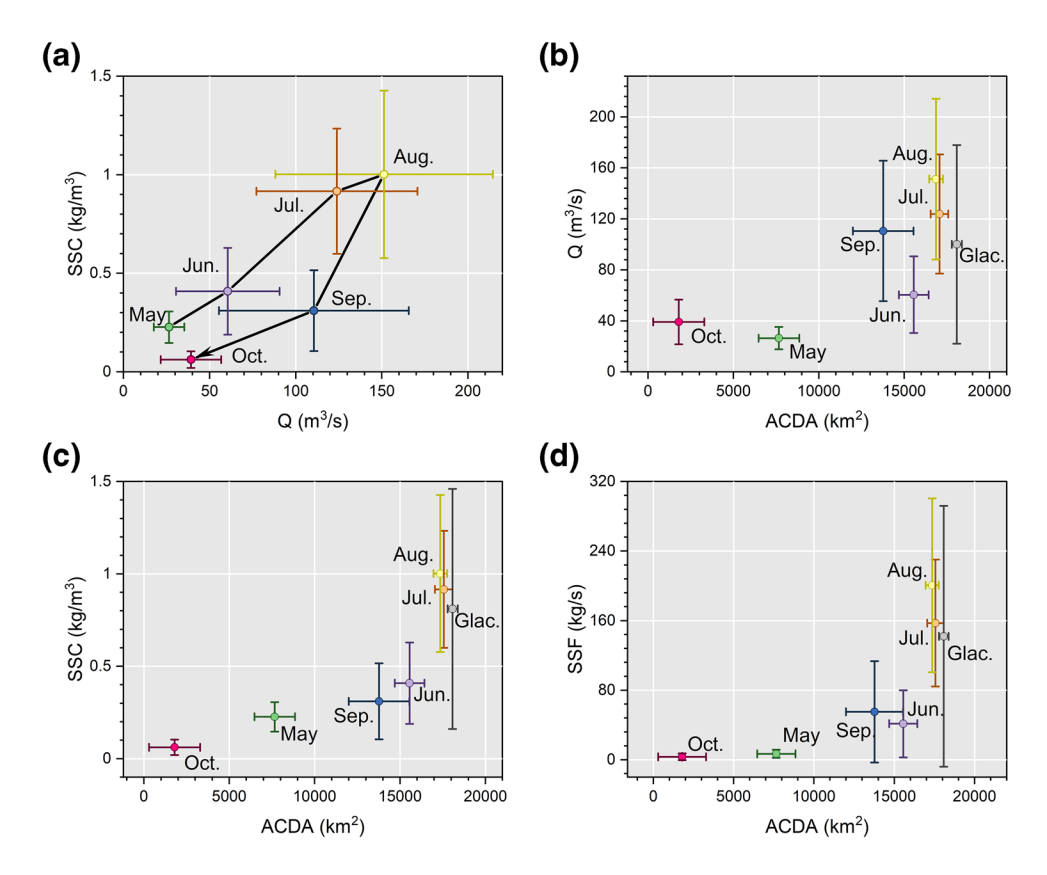


Figure 6. Monthly variations in *Q*, SSC, active contributing drainage area (ACDA), and their relations. (a) Mean monthly hysteresis between discharge and SSC, showing a clockwise pattern from May to October as is considered typical for a sediment supply limited system. (b–d) *Q*, SSC, and SSF generally increase as a function of ACDA. In (c) and (d), the substantial increases in the SSC and SSF from June to July–August suggests the significant contributions from glacial erosion and permafrost processes. Glac. denotes the period of glacier melt days, when the glacier landscape is active for runoff and sediment generations (the days when the freezing line altitude is above the glacier terminus at 5,500 m a.s.l.). *Q*, Discharge; SSC, suspended sediment concentration.

and Supplement Figures S4 and S5). Both air temperature and ACDA exhibit a significant correlation with SSC (Figure 6c and Supplement Figure S4b). In spring from May to June, the air temperature gradually rises above 0°C and increases the ACDA (Figure 8). The rise in temperature and expansion of ACDA allows for snowmelt runoff generation associated with snowpack melting (Figure 8b). Since the snowmelt runoff is unlikely to infiltrate into the largely frozen subsurface (Woo & McCann, 1994; Y. Wu et al., 2018), it mobilizes the shallowest surface sediment (including sediment in or on snow) and increases riverine SSCs. The relatively small SSCs in spring (SSC $< 0.5 \text{ kg/m}^3$) correlate well with the ACDAs as $\sim 60\%$ of the catchment during this period is classified as erodible landscape that are active for runoff and sediment generation (Figure 6c). In summer (from July to August), the highest discharges, SSCs, and SSFs in a hydrological year are observed, which is accompanied by the largest ACDA and highest temperature (Figures 6 and 8). The ACDA reaches its maximum in summer and engages the upstream glaciers at altitudes above 5,500 m a.s.l. (this occurs when temperature at the TTH station (4,500 m a.s.l.) is above 6°C), which produces both glacial runoff and sediment to the downstream. Degree-day glacier melt models estimate the ratio of glacier melt runoff to the total annual runoff ranges from 4% to 11% (Shiyin et al., 2009; Q. Wang, Zhang, et al., 2017). Thus, the sediment component from glacial erosion to the total annual sediment flux is estimated to be 6%-15% based on the discharge-SSC relation in summer (Figure 5d). However, this number may be underestimated as sediment yields in glaciated basins are often much higher than those unglaciated basins (Hallet et al., 1996).

Furthermore, permafrost processes significantly contribute to the runoff and sediment production and transport in summer (Figure 8). Stable isotope analysis in the TTH basin shows that supra-permafrost groundwater contributes \sim 50% of the total annual runoff, with glacier-snow melt accounting for \sim 25% and

LI ET AL. 8 of 14

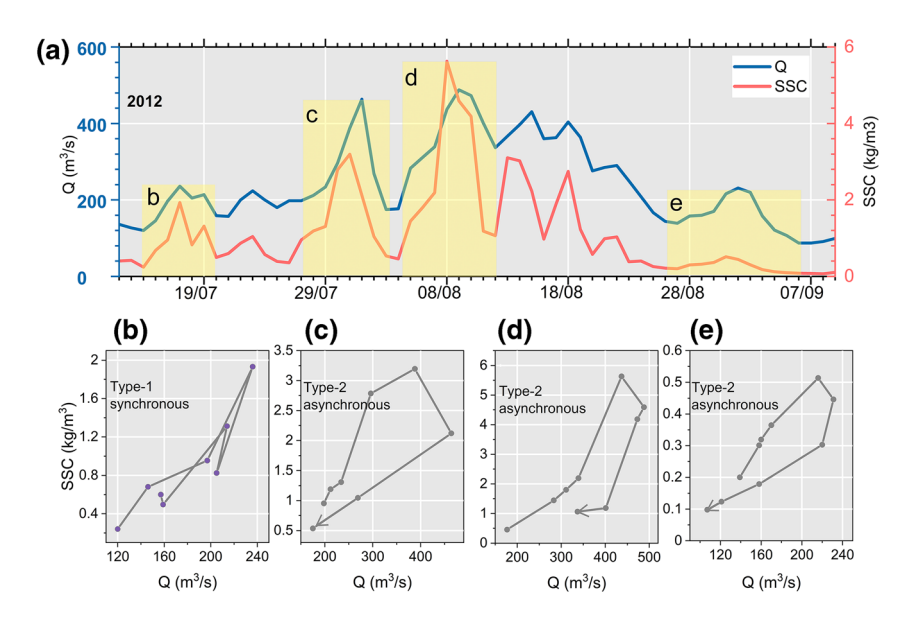


Figure 7. Hydrograph and discharge-SSC hysteresis patterns using 2012 as an example. (a) The hydrographs of discharge and SSC for four successive floods (the yellow and gray shaded). Note that the SSCs during the fourth flood (the gray shaded) are very small although the discharges are comparable to the first flood. This is due to the limited availability of sediment in the autumn recession season. (b–e) The discharge-SSC hysteresis patterns of the four successive floods. The hysteresis pattern changes from an approximate synchronous pattern to clockwise asynchronous patterns, suggesting a sediment supply limited system. SSC, suspended sediment concentration.

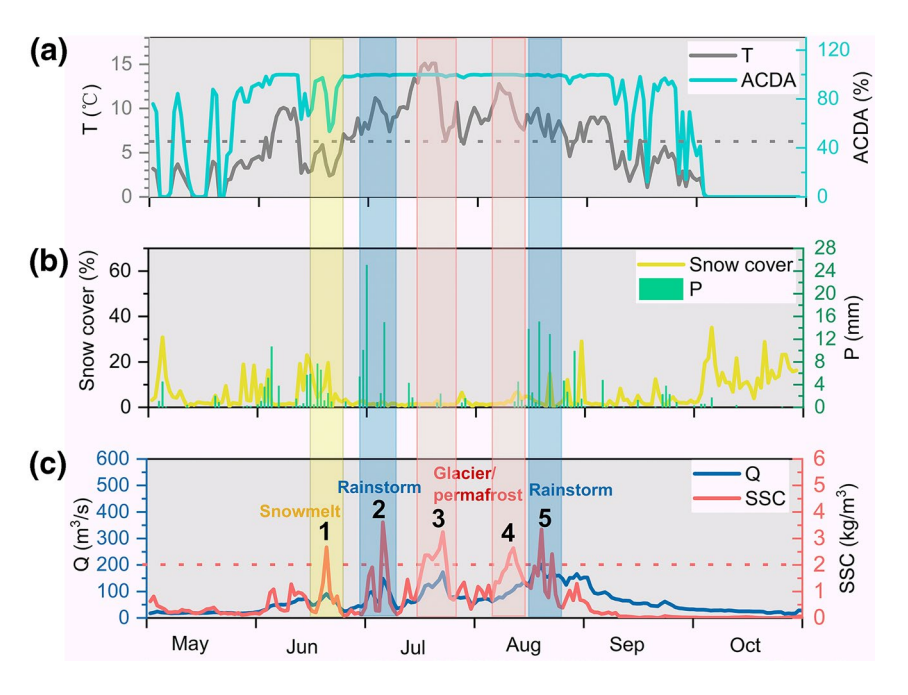


Figure 8. Daily Q and SSC controlled by air temperature (T), active contributing drainage area (ACDA), snow cover, precipitation (P), and glacier-permafrost processes in the hydrological year of 2006. The first SSC pulse (SSC > 2 kg/m³) in June is caused by snowmelt. The second and fifth SSC pulses are induced by rainstorms (P > 15 mm or the top one percentile, see Supplement Figure S4). The third and fourth SSC pulses are due to glacial contributions and (or) permafrost processes (e.g., thaw slumps). Q, Discharge; SSC, suspended sediment concentration.

LI ET AL. 9 of 14

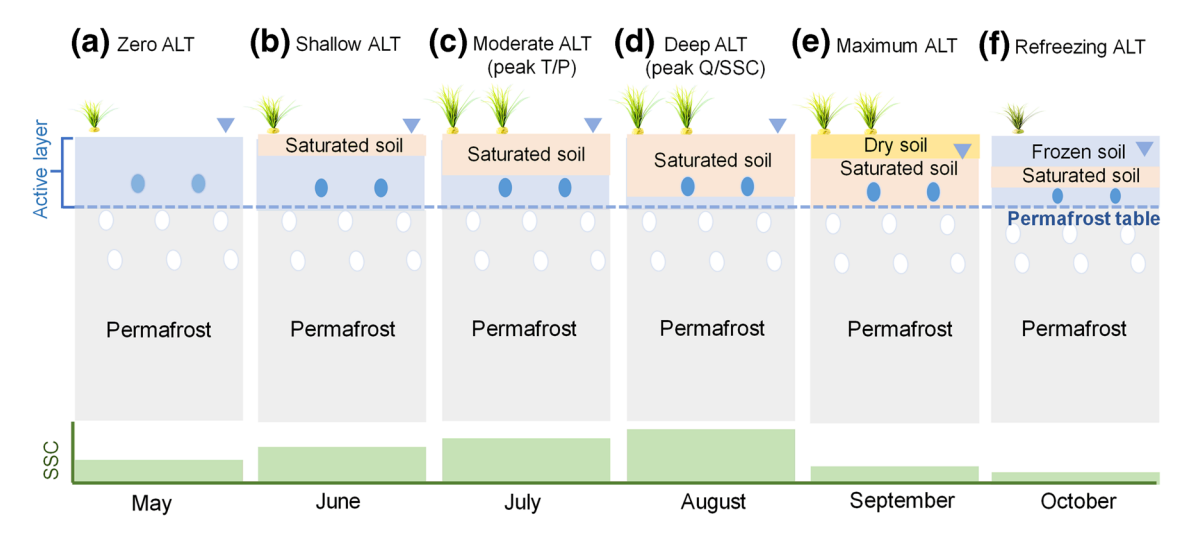


Figure 9. Conceptual diagram depicting the impact of active layer freeze-thaw cycle on *Q* and SSC. ALT = active layer thickness. The blue triangles, blue granules, and white granules denote the water tables, supra-permafrost aquifer, and ground-ice, respectively. The blue-gray line denotes the permafrost table. The heights of the bottom green panels represent the median SSCs of each month on a relative scale. (a) In early spring (May), the majority of the basin is still frozen, see also Figure 3b. (b) In June when the thaw cycle starts, the ALT is still shallow due to the low temperature. (c and d) In summer, the ALT continues to increase with rising temperature. From July to August, the *Q* continues to increase due to the increased runoff component from supra-permafrost aquifer. (e) In September when the ALT reaches its maximum, the water table drops and surface soil becomes dry, reducing surface runoff. (f) In October when the freeze cycle begins, the ALT shows a two-way decline (i.e., from top to bottom and from bottom to top). The ALT and seasonal soil moisture changes are based on the field observed data in a similar continuous permafrost basin on the Tibetan Plateau (Q. Wang, Zhang, et al., 2017). *Q*, Discharge; SSC, suspended sediment concentration.

rainfall for \sim 25%, respectively (Z. Li, Li, Feng, et al., 2020). In autumn when the active layer thickness reaches its maximum and surfaces runoff decreases substantially, the supra-permafrost groundwater can provide 70%–90% of the runoff (Z. Li, Li, Feng, et al., 2020; G. Wang et al., 2009). Permafrost disturbances (e.g., thaw slumps, Figure 2c) that are coupled with river networks can deliver considerable amounts of fine-grained fluvial sediments into the river channel (Kokelj et al., 2013; Rudy et al., 2017). Thaw slumps in ice-rich permafrost basins are especially active in summer and have increased due to climate warming in the headwater region of the Yangtze River (Figure S7) and also other places of the TP (Huang et al., 2020; Luo et al., 2019; Mu et al., 2020). Thaw slumps can be trigged by ground-ice exposure and ablation due to extreme thaw or fluvial-thermal erosion (Luo et al., 2019). The accumulated materials, highly weatherable fine-grained sediment, at the slump toes are further transported downslope by the ground-ice melt water to affect streams (Kokelj et al., 2013). It is also possible that sediments from the disturbed permafrost slopes are temporarily stored in the river systems (e.g., channels, braided bars, and floodplains) that offset the increased signal at the basin outlet (Beel et al., 2018). However, in the medium-sized TTH basin, \sim 18,000 km², the increased sediment supplies from permafrost slopes are clearly detected at a 33-year timescale (Figure 4d).

Additionally, the seasonal evolution of the active layer also affects discharge and SSC dynamics (Figure 9). For instance, the mean monthly discharge and SSC peak in August (Figure 6a), although the temperature and precipitation peak in July (Figure 1d). The increase in discharge from July to August may primarily result from the supra-permafrost aquifers that are released via new subsurface flow pathways and water tracks along with continual increasing of the active layer thickness (Evans et al., 2020; Z. Li, Li, Feng, et al., 2020; G. Wang et al., 2009). The increased discharge in August further increases SSCs and SSFs likely through fluvial channel erosion. In September when the active layer thickness reaches its maximum associated with continuous above 0°C temperature, the top soil can become dry as a result of a drop of the water table (Q. Wang, Zhang, et al., 2017). This results in high baseflow (70%–90% of the total runoff) and very low surface flow (G. Wang et al., 2009), restricting surface flow erosion and leading to the very low SSC. For instance, for the four successive floods in 2012, the SSCs during the fourth flood (early September) are very small although the water discharges are comparable to the first flood (July; Figure 7). In October, the freeze cycle starts and the ACDA decreases dramatically (ACDA in percentage is less than 10%), restricting the erodible landscape and decreasing both discharge and SSC significantly (Figures 6 and 8).

LI ET AL. 10 of 14

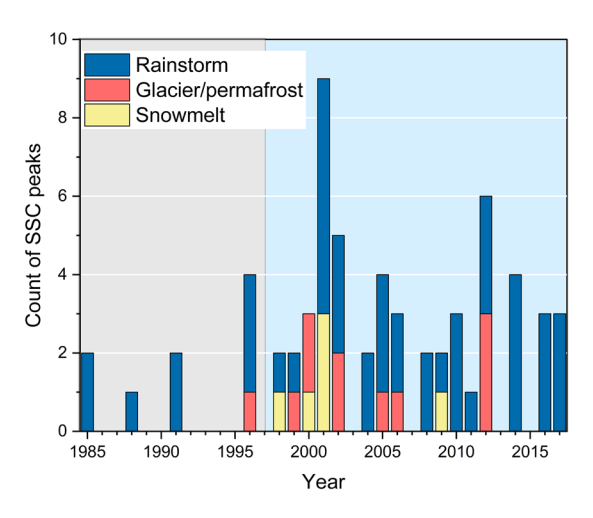


Figure 10. Different drivers of peak SSC events from 1985 to 2017. Rainstorm (i.e., rainfall > 15 mm, the top one percentile) is the major driver of the SSC peaks (i.e., SSC > 2.90 kg/m³, the top one percentile), followed by glacier/permafrost processes and snowmelt, respectively. Glacier/permafrost melt processes are invoked when SSC peaks occur without rainstorms in the previous 3 days. SSC, suspended sediment concentration.

4.2. Pluvial Control

We find that rainstorms often determine the peak SSC events (i.e., $SSC > 2.90 \text{ kg/m}^3$) in the TTH basin (Figure 10). Over the last 3 decades, 46 of the 63 peak SSC events can be attributed to rainstorms, followed by glacier/permafrost melt (11 times) and snowmelt (6 times), respectively. Furthermore, more frequent rainstorm-driven peak SSC events occurred in the period of 1998-2017, relative to the baseline period of 1985-1997. For instance, the rainstorm with 61 mm during a 7-day period prior to the peak flow generated a historical record peak of SSC of 7.43 kg/m³ (7,430 mg/l) on July 29, 2008 (Figure S6). As a result, 67% of the total annual sediment flux and 17% of the total annual runoff were transported within the seven days from 26 July to 1 August. In permafrost basins, rainstorms in summer can contribute to peak SSC events via both conventional slope processes and exacerbation of thaw slumps (Beel et al., 2018; Kokelj et al., 2013, 2015). On the one hand, rainstorms often trigger slope wash and mass wasting (e.g., landslides and debris flows) and enhance fluvial channel erosion because of the increased discharge (Beylich et al., 2017; Wulf et al., 2012). On the other hand, rainstorms promote thaw slump growth and the evolution of small-scale slumps into mega-scale slumps; because rainstorms accompanied with the slump ground-ice meltwater can perpetuate the evacuation of the accumulated materials and promote the gullying of the scar zone (Kokelj et al., 2013).

4.3. Future River Dynamics in Permafrost-Dominated Basins of the TP

Various climate projections show a warmer and wetter future accompanied by more frequent extreme weather events for most headwater regions of the TP (IPCC, 2019). For instance, the IPCC's Representative Concentration Pathway 4.5 and 8.5 scenarios project a warming of 3.5° C \pm 0.2° C and 6.0° C \pm 0.3° C for the region by the end of this century, a much faster warming rate than the global average due to the elevation-dependent warming (Kraaijenbrink et al., 2017). A warmer climate would increase the ratio of rainfall to snowfall (Smith & Bookhagen, 2018; Yao et al., 2019) and likely decrease snowmelt runoff and snowmelt erosion. In a warming summer, the accelerating glacier melt will continue to increase glacier runoff until ~2030s, beyond which the glacier runoff likely decreases (Huss & Hock, 2018; Zhao et al., 2019). The sediment fluxes from glaciers and newly exposed proglacial and paraglacial areas may continue to rise for decades to centuries after ~2030s (Church & Ryder, 1972); because landscapes after deglaciation are prone to slope failures during rainfall events and would greatly enhance sediment supplies due to losing the buttressing effects of ice (Church & Ryder, 1972; Orwin & Smart, 2004).

In a warming and wetting climate, permafrost thaw slumps and thermal gullies will also accelerate in the TP (Supplement Figure S7, Luo et al., 2019) and couple with downstream river networks; this will very likely increase sediment sources and fluvial sediment loads in summer (Supplement Figure S8) (Kokelj et al., 2013; Rudy et al., 2017). The frequency and magnitude of the permafrost disturbances can also be exacerbated by more frequent rainstorms (Kokelj et al., 2013), increasing peak fluvial events (Figure 11). Observations in the High Arctic indicate that increased erosion and sediment production from permafrost thaw disturbances occur more rapidly than reductions in surface runoff associated with deeper active layer (Rowland et al., 2010).

Furthermore, a warmer climate will increase the ACDA particularly in spring and autumn, thus allowing expanding erodible landscapes for the aforementioned thermal and pluvial processes and enhancing discharges and sediment fluxes (Figure 4 and Supplement Figure S8). Overall, for similar permafrost river basins on the TP like the TTH basin, we predict that the fluvial sediment fluxes will continue to increase along with more frequent extreme events in a warmer and wetter future. The rising fluvial sediment fluxes from permafrost basins have important implications for the downstream hydropower dams and riverine biogeochemical cycles (Beel et al., 2020; D. Li et al., 2018; D. Li, Li, Zhou, et al., 2020; Song et al., 2020).

LI ET AL. 11 of 14

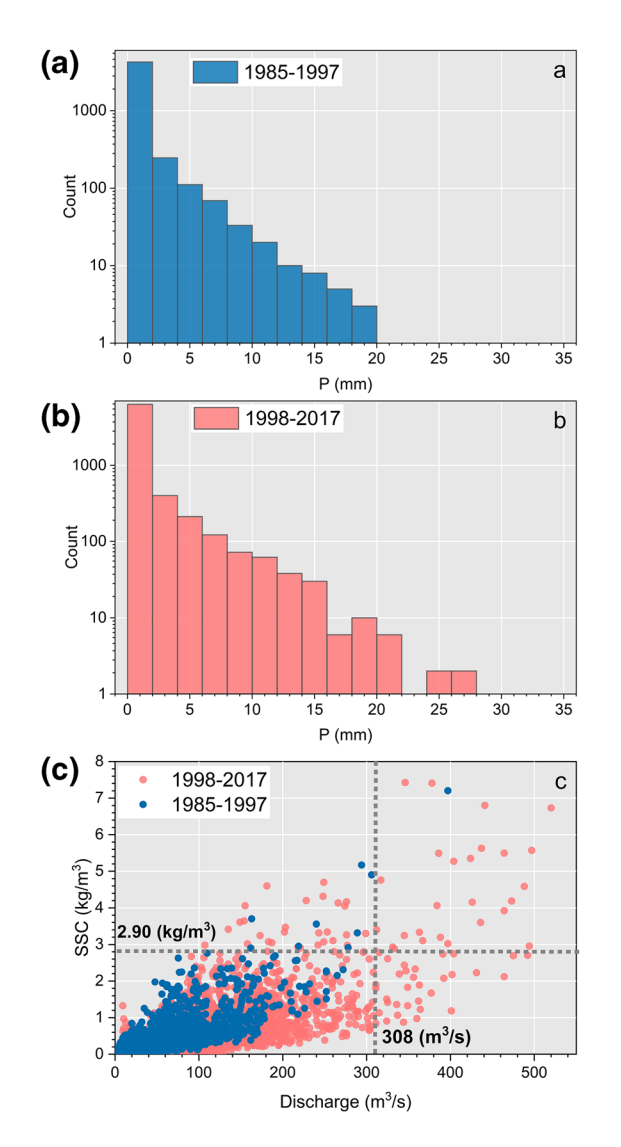


Figure 11. Higher frequency in rainstorms in recent years corresponds well to the more frequent peak discharge-SSC events. Rainstorms (P > 15 mm; the top 1 percentile) have clearly increased during 1998–2017 (43 days), relative to 1985–1997 (17 days). Almost all peak SSC-discharge events (discharge > 308 m 3 /s and the SSC > 2.90 kg/m 3 , i.e., the top 1 percentile) are recorded in the more recent years (e.g., 1998–2017). SSC, suspended sediment concentration.

5. Conclusions

This study examines the response of discharge and sediment regimes to climate, erodible landscape, and active layer freeze-thaw in a high-altitude permafrost-dominated basin on the Tibetan Plateau across multiple timescales. In response to climate warming, the erodible landscape (defined as the ACDA) in this region is expanding rapidly and the fluvial water and sediment fluxes are increasing substantially over the investigation period from 1985 to 2017. In particular, the sediment fluxes have more than doubled. At the seasonal timescale, air temperature determines discharge and suspended sediment concentration dynamics by controlling the evolving erodible landscape and multiple thermal-driven processes within catchments (i.e., snowmelt in spring and glacier melt and permafrost processes in summer). The temperature-driven seasonal active layer freeze-thaw cycle also influences discharge and sediment dynamics. For instance, the maximum active layer thickness in September corresponds to the dominant supra-permafrost groundwater runoff in the autumn recession season, which likely restricts surface flow erosion and leads to the relatively high total discharge but very low sediment concentration in this period. In addition, most of the peak sediment concentration events are caused by rainstorms possibly through slope wash, mass wasting, and exacerbation of permafrost thaw slumps. In a warming and wetting future, we expect that the fluvial sediment fluxes will continue to increase and there would be more frequent fluvial extreme events along with the expanding erodible landscapes and the intensifying thermal and pluvial-driven processes such as thaw slumps.

Given that a significant portion of the Tibetan Plateau is underlain by continuous permafrost, this study suggests that permafrost thaw on the TP plays a more important role in driving the water and sediment dynamics than previous thought (Huss & Hock, 2018; Immerzeel et al., 2010) and thus should be considered as an important driver of water and sediment changes in the past and future. These findings have important implications for assessing the fluvial responses to permafrost thaw in other ungauged parts of the entire Tibetan Plateau and evaluating the downstream impacts on river channel dynamics, hydropower development and operations, water quality, flooding, and aquatic ecosystems. Our insights also underline the need for more permafrost-hydrology observations across the region in order to better assess the impacts of changing permafrost landscapes on fluvial systems in the context of climate change.

Data Availability Statement

Precipitation and air temperature data are retrieved from the National Meteorological Information Center, China Meteorological Administration (CMA) (http://data.cma.cn/en). Discharge and sediment data are sourced and available from the Qinghai Hydrology Bureau and the Changjiang Water Resources Commission (http://www.cjh.com.cn/en/). The land use and land cover data are obtained from the GlobeLand30 data set (http://www.globallandcover.com). The Normalized Difference Vegetation Index (NDVI) data are derived from the Land Processes Distributed Active Archive Center, NASA (https://lpdaac.usgs.gov/). The snow cover data are derived from the MODIS Terra/Aqua Snow Cover Daily L3 Global 500-m Grid (MO/YD10A1) data set (https://nsidc.org/data/MOD10A1). Other data such as basin boundary, river networks, and DEM are available at the National Tibetan Plateau Data Center (http://www.tpdc.ac.cn/en/). Source data of key figures can also be found in https://blog.nus.edu.sg/geolidf/data-sharing/.

LI ET AL. 12 of 14



Acknowledgments

This study was supported by the National University of Singapore (R-109-000-227-115), the MOE Tier 2 Grant (T2EP50120-0030), and the Central Public-interest Scientific Institution Basal Research Fund (CKSF2019292). Dongfeng Li acknowledges IPCC Scholarship Award (jointly founded by the IPCC and Cuomo Foundation) and President's Graduate Fellowship. Irina Overeem acknowledges NSF OPP award 1553172. We much appreciate Professor Tom Dunne for his critical evaluation and comment on the earlier version of the manuscript. We also thank Professor Bob Wasson for the discussion on the sediment sources.

References

- Beel, C. R., Lamoureux, S. F., & Orwin, J. F. (2018). Fluvial response to a period of hydrometeorological change and landscape disturbance in the Canadian High Arctic. *Geophysical Research Letters*, 45(19), 10446–10455. https://doi.org/10.1029/2018GL079660
- Beel, C. R., Lamoureux, S. F., Orwin, J. F., Pope, M. A., Lafrenière, M. J., & Scott, N. A. (2020). Differential impact of thermal and physical permafrost disturbances on High Arctic dissolved and particulate fluvial fluxes. *Scientific Reports*, 10(1), 11836.
- Best, J. (2019). Anthropogenic stresses on the world's big rivers. Nature Geoscience, 12(1), 7-21.
- Beylich, A. A., Laute, K., & Storms, J. E. A. (2017). Contemporary suspended sediment dynamics within two partly glacierized mountain drainage basins in western Norway (Erdalen and Bødalen, inner Nordfjord). *Geomorphology*, 287, 126–143.
- Biskaborn, B. K., Smith, S. L., Noetzli, J., Matthes, H., Vieira, G., Streletskiy, D. A., & Lantuit, H. (2019). Permafrost is warming at a global scale. *Nature Communications*, 10(1), 264.
- Brun, F., Berthier, E., Wagnon, P., Kääb, A., & Treichler, D. (2017). A spatially resolved estimate of High Mountain Asia glacier mass balances from 2000 to 2016. *Nature Geoscience*, 10(9), 668–673.
- Church, M., & Ryder, J. M. (1972). Paraglacial sedimentation: A consideration of fluvial processes conditioned by glaciation. Geological Society of America Bulletin, 83(10), 3059–3072.
- Colgan, P. M., Munroe, J. S., & Shangzhe, Z. (2006). Cosmogenic radionuclide evidence for the limited extent of last glacial maximum glaciers in the Tanggula Shan of the Central Tibetan Plateau. *Quaternary Research*, 65(02), 336–339.
- Delaney, I., & Adhikari, S. (2020). Increased subglacial sediment discharge in a warming climate: Consideration of ice dynamics, glacial erosion, and fluvial sediment transport. *Geophysical Research Letters*, 47(7), e2019G–e85672G. https://doi.org/10.1029/2019GL085672
- Dietrich, W. E., & Dunne, T. (1978). Sediment budget for a small catchment in Mountainous Terrain. Zietschrift Fur Geomorphologie, 29,
- Dunne, T., & Black, R. D. (1970). An experimental investigation of runoff production in permeable soils. *Water Resources Research*, 6(2), 478–490.
- Evans, S. G., Godsey, S. E., Rushlow, C. R., & Voss, C. (2020). Water tracks enhance water flow above permafrost in upland Arctic Alaska hillslopes. *Journal of Geophysical Research: Earth Surface*, 125(2), e2019J-e5256J. https://doi.org/10.1029/2019JF005256
- Gunawardhana, L. N., & Kazama, S. (2012). A water availability and low-flow analysis of the Tagliamento River discharge in Italy under changing climate conditions. *Hydrology and Earth System Sciences Discussions*, 9(1), 139–173.
- Hallet, B., Hunter, L., & Bogen, J. (1996). Rates of erosion and sediment evacuation by glaciers: A review of field data and their implications, Global and Planetary Change, 12(1-4), 213-235.
- Huang, L., Luo, J., Lin, Z., Niu, F., & Liu, L. (2020). Using deep learning to map retrogressive thaw slumps in the Beiluhe region (Tibetan Plateau) from CubeSat images. *Remote Sensing of Environment*, 237, 111534.
- Huss, M., & Hock, R. (2018). Global-scale hydrological response to future glacier mass loss. Nature Climate Change, 8(2), 135-140.
- Immerzeel, W. W., Lutz, A. F., Andrade, M., Bahl, A., Biemans, H., Bolch, T., & Baillie, J. E. M. (2020). Importance and vulnerability of the world's water towers. *Nature*, 577(7790), 364–369.
- Immerzeel, W. W., van Beek, L. P. H., & Bierkens, M. F. P. (2010). Climate change will affect the Asian water towers. *Science*, 328(5984), 1382–1385.
- IPCC. (2019). Special report on the ocean and cryosphere in a changing climate. Monaco: IPCC.
- Kokelj, S. V., Lacelle, D., Lantz, T. C., Tunnicliffe, J., Malone, L., Clark, I. D., & Chin, K. S. (2013). Thawing of massive ground ice in mega slumps drives increases in stream sediment and solute flux across a range of watershed scales. *Journal of Geophysical Research: Earth Surface*, 118(2), 681–692. https://doi.org/10.1002/jgrf.20063
- Kokelj, S. V., Tunnicliffe, J., Lacelle, D., Lantz, T. C., Chin, K. S., & Fraser, R. (2015). Increased precipitation drives mega slump development and destabilization of ice-rich permafrost terrain, northwestern Canada. *Global and Planetary Change*, 129, 56–68.
- Koppes, M., Hallet, B., Rignot, E., Mouginot, J., Wellner, J. S., & Boldt, K. (2015). Observed latitudinal variations in erosion as a function of glacier dynamics. *Nature*, 526(7571), 100–103.
- Kraaijenbrink, P. D. A., Bierkens, M. F. P., Lutz, A. F., & Immerzeel, W. W. (2017). Impact of a global temperature rise of 1.5 degrees Celsius on Asia's glaciers. *Nature*, 549(7671), 257–260.
- Lane, S. N., Bakker, M., Gabbud, C., Micheletti, N., & Saugy, J. (2017). Sediment export, transient landscape response and catchment-scale connectivity following rapid climate warming and Alpine glacier recession. *Geomorphology*, 277, 210–227.
- Li, Z., Li, Z., Feng, Q., Zhang, B., Gui, J., Xue, J., & Gao, W. (2020). Runoff dominated by supra-permafrost water in the source region of the Yangtze river using environmental isotopes. *Journal of Hydrology*, 582, 124506.
- Li, D., Li, Z., Zhou, Y., & Lu, X. (2020). Substantial increases in the water and sediment fluxes in the headwater region of the Tibetan Plateau in response to global warming. *Geophysical Research Letters*, 47(11), e2020G–e87745G. https://doi.org/10.1029/2020GL087745
- Li, D., Lu, X. X., Yang, X., Chen, L., & Lin, L. (2018). Sediment load responses to climate variation and cascade reservoirs in the Yangtze River: A case study of the Jinsha River. Geomorphology, 322, 41–52.
- Li, Y., Wang, C., Ma, C., Xu, G., & Zhao, X. (2011). Balanced cross-section and crustal shortening analysis in the Tanggula-Tuotuohe Area, Northern Tibet. *Journal of Earth Science*, 22(1), 1–10.
- Luo, J., Niu, F., Lin, Z., Liu, M., & Yin, G. (2019). Recent acceleration of thaw slumping in permafrost terrain of Qinghai-Tibet Plateau: An example from the Beiluhe Region. *Geomorphology*, 341, 79–85.
- Lu, X. X., Zhang, S., & Xu, J. (2010). Climate change and sediment flux from the Roof of the World. Earth Surface Processes and Landforms, 35(6), 732–735.
- Milliman, J. D., & Syvitski, J. P. M. (1992). Geomorphic/tectonic control of sediment discharge to the ocean: The importance of small mountainous rivers. *Journal of Geology*, 100(5), 525–544.
- Mu, C., Shang, J., Zhang, T., Fan, C., Wang, S., Peng, X., & Jia, L. (2020). Acceleration of thaw slump during 1997–2017 in the Qilian Mountains of the northern Qinghai-Tibetan plateau. *Landslides*, 17(5), 1051–1062.
- Orwin, J. F., & Smart, C. C. (2004). The evidence for paraglacial sedimentation and its temporal scale in the deglacierizing basin of Small River Glacier, Canada. *Geomorphology*, 58(1–4), 175–202.
- Overeem, I., Hudson, B. D., Syvitski, J. P. M., Mikkelsen, A. B., Hasholt, B., van den Broeke, M. R., & Morlighem, M. (2017). Substantial export of suspended sediment to the global oceans from glacial erosion in Greenland. *Nature Geoscience*, 10(11), 859–863.
- Pettitt, A. N. (1979). A non-parametric approach to the change-point problem. *Applied Statistics*, 28, 126–135.
- Rowland, J. C., Jones, C. E., Altmann, G., Bryan, R., Crosby, B. T., Hinzman, L. D., & Marsh, P. (2010). Arctic landscapes in transition: Responses to thawing permafrost. Eos, Transactions American Geophysical Union, 91(26), 229–230. https://doi.org/10.1029/2010EO260001

LI ET AL. 13 of 14



- Rudy, A. C. A., Lamoureux, S. F., Kokelj, S. V., Smith, I. R., & England, J. H. (2017). Accelerating thermokarst transforms ice-cored terrain triggering a downstream cascade to the ocean. *Geophysical Research Letters*, 44(21), 11080–11087. https://doi.org/10.1002/2017GL074912 Shiyin, L., Yong, Z., Yingsong, Z., & Yongjian, D. (2009). Estimation of glacier runoff and future trends in the Yangtze River source region, China. *Journal of Glaciology*, 55(190), 353–362.
- Smith, T., & Bookhagen, B. (2018). Changes in seasonal snow water equivalent distribution in High Mountain Asia (1987 to 2009). Science Advances, 4(1), e1701550.
- Song, C., Wang, G., Haghipour, N., & Raymond, P. A. (2020). Warming and monsoonal climate lead to large export of millennial-aged carbon from permafrost catchments of the Qinghai-Tibet Plateau. *Environmental Research Letters*, 15(7), 74012.
- Syvitski, J. P. (2002). Sediment discharge variability in Arctic rivers: Implications for a warmer future. Polar Research, 21(2), 323-330.
- Walling, D. E. (2006). Human impact on land-ocean sediment transfer by the world's rivers. Geomorphology, 79(3-4), 192-216.
- Wang, G., Hu, H., & Li, T. (2009). The influence of freeze-thaw cycles of active soil layer on surface runoff in a permafrost watershed. *Journal of Hydrology*, 375(3–4), 438–449.
- Wang, G., Liu, G., & Liu, L. (2012). Spatial scale effect on seasonal streamflows in permafrost catchments on the Qinghai-Tibet Plateau. Hydrological Processes, 26(7), 973–984.
- Wang, T., Yang, D., Yang, Y., Piao, S., Li, X., Cheng, G., & Fu, B. (2020). Permafrost thawing puts the frozen carbon at risk over the Tibetan Plateau. Science Advances, 6(19), z3513.
- Wang, R., Yao, Z., Wu, S., & Liu, Z. (2017). Glacier retreat and its impact on summertime run-off in a high-altitude ungauged catchment. Hydrological Processes, 31(21), 3672–3681.
- Wang, Q., Zhang, T., Jin, H., Cao, B., Peng, X., Wang, K., & Cao, L. (2017). Observational study on the active layer freeze–thaw cycle in the upper reaches of the Heihe River of the north-eastern Qinghai-Tibet Plateau. *Quaternary International*, 440, 13–22.
- Woo, M., & McCann, B. S. (1994). Climatic variability, climatic change, runoff, and suspended sediment regimes in northern Canada. *Physical Geography*, 15(3), 201–226.
- Wulf, H., Bookhagen, B., & Scherler, D. (2012). Climatic and geologic controls on suspended sediment flux in the Sutlej River Valley, western Himalaya. *Hydrology and Earth System Sciences*, 16(7), 2193–2217.
- Wu, Y., Ouyang, W., Hao, Z., Yang, B., & Wang, L. (2018). Snowmelt water drives higher soil erosion than rainfall water in a mid-high latitude upland watershed. *Journal of Hydrology*, 556, 438–448.
- Wu, W., Xu, S., Lu, H., Yang, J., Yin, H., & Liu, W. (2011). Mineralogy, major and trace element geochemistry of riverbed sediments in the headwaters of the Yangtze, Tongtian River and Jinsha River. *Journal of Asian Earth Sciences*, 40(2), 611–621.
- Yao, T., Xue, Y., Chen, D., Chen, F., Thompson, L., Cui, P., & Mosbrugger, V. (2019). Recent Third Pole's rapid warming accompanies cryospheric melt and water cycle intensification and interactions between monsoon and environment: Multidisciplinary approach with observations, modeling, and analysis. *Bulletin of the American Meteorological Society*, 100(3), 423–444.
- Zhang, F., Shi, X., Zeng, C., Wang, L., Xiao, X., Wang, G., & Immerzeel, W. (2020). Recent stepwise sediment flux increase with climate change in the Tuotuo River in the central Tibetan Plateau. Science Bulletin, 65(5), 410–418.
- Zhao, Q., Ding, Y., Wang, J., Gao, H., Zhang, S., Zhao, C., et al. (2019). Projecting climate change impacts on hydrological processes on the Tibetan Plateau with model calibration against the glacier inventory data and observed streamflow. *Journal of Hydrology*, 573, 60–81.

LI ET AL. 14 of 14